

The non-linearity between $\langle \ln A \rangle$ and $\langle X_{\max} \rangle$ induced by the acceptance of fluorescence telescopes

R. Ulrich^b, L. Cazon^{a,*}

^a*LIP, Av. Elias Garcia, 14-1, 1000-149 Lisboa, Portugal*

^b*Institut für Kernphysik, Postfach 3640, 76021 Karlsruhe, Germany*

Abstract

The measurement of the average depth of the shower maximum is the most commonly used observable for the possible inference of the primary cosmic-ray mass composition. Currently, different experimental Collaborations process and present their data not in the same way, leading to problems in the comparability and interpretation of the results. Whereas $\langle X_{\max} \rangle$ is expected to be proportional to $\langle \ln A \rangle$ in ideal conditions, we demonstrate that the finite field-of-view of fluorescence telescopes plus the attenuation in the atmosphere introduce a non-linearity into this relation, which is specific for each particular detector setup.

Keywords: cosmic-rays, extensive air-showers, shower maximum, telescope, field-of-view

1. Introduction

Ultra-high energy cosmic-ray (UHECR) particles are the highest energy particles observed by humankind, well beyond what is accessible at the Large Hadron Collider. Current experiments [1, 2, 3] are recording large amounts of high quality data. Recent observations do not draw a simple nor consistent picture of the nature of UHECR particles. There are hints of anisotropy in the arrival directions [4], favouring the presence of light primary particles. Using the current high energy hadronic interaction models, typical air-shower observables do not generally support the light component hypothesis: the Pierre

*Corresponding author *Tel* +351 217973880 *Fax* +351 217934631
Email address: cazon@lip.pt (L. Cazon)

Auger Collaboration observes the depth of the electromagnetic shower maximum, muon production maximum, rise-time of the shower front, etc. that are all pointing in the direction of a primary composition dominated by heavy particles at ultra-high energies [5, 6]. On the other hand, the HiRes Collaboration claims that their measurement of the depth of the shower maximum is compatible with protons up to the highest energies [7], which is currently supported by the first TA data [8, 9]. It is important to notice that whereas Auger publishes $\langle X_{\max} \rangle$ in the atmosphere by using a fiducial volume selection to minimize acceptance biases, HiRes and TA presently do not apply such corrections and present $\langle X_{\max} \rangle$ at the detector level. Also the possible difference of the energy scale between Auger and HiRes/TA ($\approx 25\%$) [10] contribute to the difficulties to explain the data [11, 12].

The current situation could point to exciting physics aspects that are about to emerge with higher accumulated event statistics, as for instance, systematic differences of the cosmic-ray flux on the northern and southern hemisphere. The Pierre Auger Observatory observes the southern, while HiRes/TA the northern sky, with very different astrophysical objects in their direct field-of-view. It is clear, that the understanding of the primary mass composition of UHECR is one of the major steps towards the final solution of the UHECR puzzle. Depending on a reliable measurement of the mass composition very different scenarios of the nature of UHECR will finally emerge.

In this article we discuss the concept of *observed* versus *true* X_{\max} -distributions to finally demonstrate that the *observed* average of depth of shower maxima, $\langle X_{\max} \rangle$, can result in a non-linear relation with the average logarithm of the mass number, $\langle \ln A \rangle$, of the UHECR. These effects are very specific for a given experimental setup and have to be accounted for in order to allow a comparison or interpretation of these data.

2. Extensive Air-Showers and Fluorescence Telescope

Fluorescence telescopes measure the ultraviolet light, which is proportional to the energy deposited by the passage of the charged particles of the air-shower cascade through the atmosphere. This makes possible to reconstruct the longitudinal profile of the electromagnetic shower [13]. The atmospheric depth at which the energy deposit is maximal is the shower maximum, X_{\max} , and is related to the nature of the primary particle. At the same primary energy, primary nuclei with mass A produce air-showers with

shower maxima at different atmospheric depths. This can be approximated as [14]

$$X_{\max} \approx \lambda_{\text{int}} + \ln 2 X_0 \ln \frac{E}{A},$$

where λ_{int} is the cross-section of cosmic-ray primaries with air and $X_0 \sim 37 \text{ g/cm}^2$ is the electromagnetic radiation length in air. The structure of this equation, $X_{\max} = a + b \ln E/A$, holds also for more general considerations [15]. It has been typically used to compute the average logarithmic mass from the data of the average depth of the shower maximum

$$\langle \ln A \rangle = \frac{1}{b} [a + b \ln E - \langle X_{\max} \rangle] = \frac{1}{b} [\langle X_{\max} \rangle_p - \langle X_{\max} \rangle].$$

Thus, there is a linear dependence of the measured average shower maximum from the average mass of the cosmic-ray primary particles.

Instead of calculating $\langle \ln A \rangle$ one can also compute the component fractions in a model with two primary cosmic-ray species. This is typically done for the proton fraction f under the assumption of a simple proton/iron mixture. For this case the relation of $\langle X_{\max} \rangle$ is

$$\langle X_{\max} \rangle = f \langle X_{\max} \rangle_p + (1 - f) \langle X_{\max} \rangle_{\text{Fe}}, \quad (1)$$

which is linear in f .

Thus, the distinction between an admixture of different primaries or a pure primary of an intermediate mass, are indistinguishable on the base of a $\langle X_{\max} \rangle$ value alone. The resulting equivalence is

$$\langle \ln A \rangle = \frac{1}{b} [\langle X_{\max} \rangle_p - \langle X_{\max} \rangle_{\text{Fe}}] (1 - f).$$

3. The effect of the telescope acceptance

The objective of this paper is not to reproduce any particular detector configuration, but to demonstrate that the relation between $\langle X_{\max} \rangle$ and $\langle \ln A \rangle$ depends critically on the detector acceptance, which varies with the primary energy. Thus, the telescope acceptance has an impact on the interpretation of $\langle X_{\max} \rangle$ data, and in general any other momentum of the X_{\max} -distribution (see also [16]).

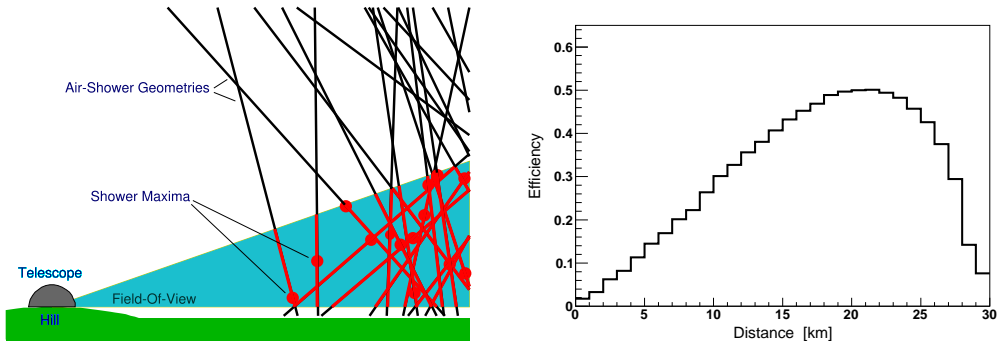


Figure 1: Left panel: Geometry of our simulation study. Right panel: Resulting efficiency, $N_{\text{obs}}/N_{\text{gen}}$, depending on the distance of air-shower cores from the telescope.

Fluorescence telescopes have a limited viewing angle defined by the optics. Showers falling outside the field-of-view cannot be detected. But even for observed showers the shower maximum can be outside the field-of-view of the telescope and can then not be reconstructed reliably. The angular field-of-view defines a volume in the atmosphere where showers can effectively be fully reconstructed. One of the most important criteria of this is that the shower maximum is located within the field-of-view. This volume is depicted in Fig. 1 (left). When showers fall very close to the telescope, the transverse area of the field-of-view is small, meaning that many shallow and/or deep showers are not fully reconstructed. This effect is naturally most severe in the energy range close to the lower detection threshold for air-showers where the distance to the events is limited by the small amount of generated fluorescence light. For air-showers detected at larger distance to the telescope the geometrical field-of-view cone is much larger. However, fluorescence light can travel only a limited distance in the atmosphere before being absorbed. At some point, light emitted at the shower axis is attenuated too much and cannot be observed any more. This is responsible for the characteristic rapid drop of the efficiency as shown in Fig. 1 (right) beyond 20 km. The Rayleigh absorption rate is proportional to the density of the atmosphere, and thus depends on changing air pressure as well as on the height in the atmosphere at which a particular shower is developing. In this work we do not discuss aerosol related absorption. It is much smaller than Rayleigh absorption and to include it here does not help the argument, but just adds additional complexity.

By means of a toy Monte Carlo we reproduce all parameters relevant for the modelling of air-shower observation with fluorescence telescopes at an arbitrary primary energy. Our simulations focus on the geometric and atmospheric effects and simplifies the situation as much as possible. We do not attempt to reproduce a specific detector setup, but only want to show the inevitable impact on the interpretation of the observed data.

The geometry of our simulation is shown in Fig. 1. The vertical depth of the telescope is at $\approx 880 \text{ g/cm}^2$, which corresponds to $h=1.5 \text{ km}$, as explained below, and the opening angle of the field-of-view is 20° . We consider air-showers of fixed primary energy, with random arrival directions, sampled from $dN/d\cos\theta = \text{const}$ up to 60° zenith angle, as well as distances l from the telescope, sampled from $dN/dl \propto l$. The requirement of a particular shower to be observed is that at least $N_{\text{det}} = 100$ photons reach the telescope from the location of the shower maximum on the shower axis. The number of photons is computed as

$$N_{\text{det}} = N_{\text{ph}} A_{\text{dia}} / r^2 \exp\left(-\frac{t}{\lambda_{\text{abs}}}\right), \quad (2)$$

where N_{ph} is the number of fluorescence photons emitted at the shower maximum, $A_{\text{dia}} = 10 \text{ m}^2$ is the aperture of the telescope, r is the geometric distance, $t = \int \rho(z) d\vec{r}$ the integrated depth distance from the telescope to the location of X_{max} , and $\lambda_{\text{abs}} = 1000 \text{ g/cm}^2$ is the photon absorption length. For air showers of primary energy E_0 and a fluorescence yield of $Y_{\text{fluo}} = 5/\text{MeV}$ the number of photons emitted at X_{max} is

$$N_{\text{ph}} = \left(\frac{dE}{dX}\right)_{\text{max}} Y_{\text{fluo}} \rho c \Delta t, \quad (3)$$

where $\Delta t = 100 \text{ ns}$ is the telescope sampling time and $(dE/dX)_{\text{max}}$ is the energy deposit at the shower maximum, which is $10^{-11.77+\lg(E_0/\text{eV})} \text{ GeV cm}^2/\text{g}$ in very good approximation¹. For air showers with $E_0 = 10^{18.5} \text{ eV}$ this yields $N_{\text{ph}} \approx 2 \cdot 10^{10}$, which is the default value throughout this paper if not stated otherwise. The atmospheric density profile $\rho(z)$ is exponential with a scale height of 8 km and a pressure at the height above sea level, $h = 1.5 \text{ km}$, of the telescope of $\approx 880 \text{ g/cm}^2$.

¹This is obtained with the SIBYLL [17] interaction model.

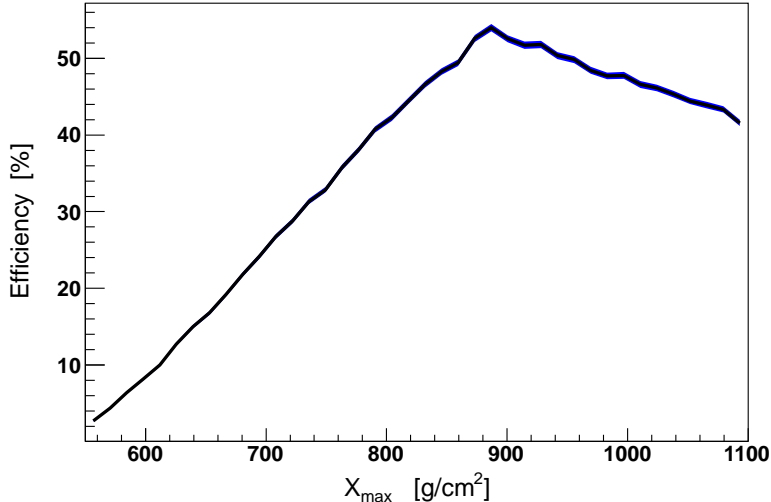


Figure 2: Efficiency $\epsilon(X_{\max})$ of the X_{\max} reconstruction as a function of X_{\max} for a particular detector, as calculated by our toy Monte Carlo.

When we generate events with a flat distribution of X_{\max} , we find that air-showers with different X_{\max} are observed with different efficiency $\epsilon(X_{\max}) = N_{\text{obs}}/N_{\text{gen}}$. In Fig. 2 we show this efficiency as a function of X_{\max} . The peak of this distribution is related to the *average atmospheric slant depth* in the volume observed by the telescope. Every telescope setup has limits both for very small as well as very large values of X_{\max} (see e.g. [18]). While large integrated atmospheric depths can in principle always be achieved by very inclined geometries, there is a strict bound on the minimal observed depth even for vertical events, which is related to the maximum possible observation distance and the upper elevation boundary of the field-of-view. This effect becomes more relevant for lower energy air-showers, since here the maximum observation distance is smaller.

Given the average efficiency $\epsilon(X_{\max})$ of a telescope setup, the measured distribution of X_{\max} is related to the parent distribution via

$$\left(\frac{dN}{dX_{\max}}\right)_{\text{measured}} = \epsilon(X_{\max}) \left(\frac{dN}{dX_{\max}}\right)_{\text{true}}.$$

Small changes in the telescope setup can yield very different $\epsilon(X_{\max})$. If also energy, X_{\max} resolution, and possible X_{\max} reconstruction biases effects were

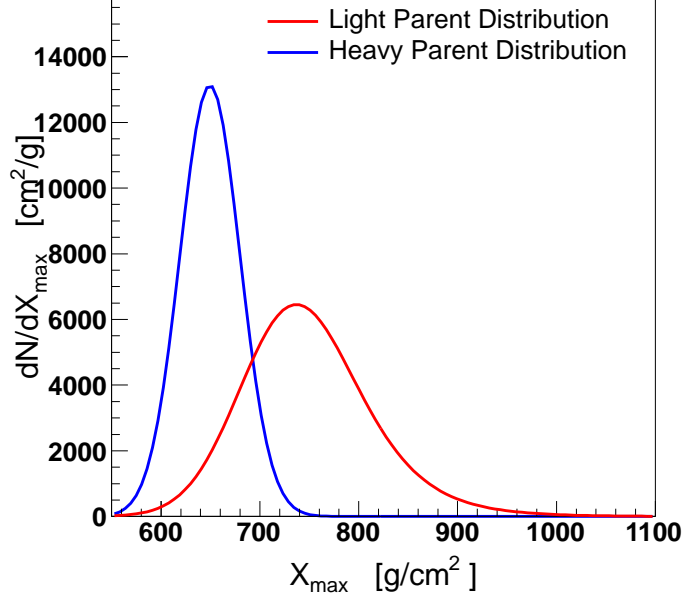


Figure 3: The two input distributions corresponding to light and heavy primary cosmic-ray particles in our study. The distributions are Exponential convoluted with a Gaussian. The used parameters of Eq. (4) are $\mu = 815 \text{ g/cm}^2$, $\sigma = 50 \text{ g/cm}^2$ and $\tau = 45 \text{ g/cm}^2$ for the light component as well as $\mu = 1005 \text{ g/cm}^2$, $\sigma = 30 \text{ g/cm}^2$ and $\tau = 5 \text{ g/cm}^2$ for the heavy component.

included the relation between the measured and parent distribution would become more complex [19, 20], but this does not help the clarity of our argument.

In the following we demonstrate how the telescope acceptance, $\epsilon(X_{\text{max}})$, affects in particular also *simple* analyses as for example related to $\langle X_{\text{max}} \rangle$. For this purpose we generate input X_{max} distributions derived from an Exponential convoluted with a Gaussian function

$$\frac{dN}{dX_{\text{max}}} = \frac{N_{\text{evt}}}{2\tau} e^{\sigma^2/(2\tau^2)} e^{(\mu - X_{\text{max}})/\tau} \text{erfc}\left(\frac{\mu - X_{\text{max}} - \sigma^2/\tau}{\sqrt{2}\sigma}\right). \quad (4)$$

In total this function has three shape parameters: the mean and width of the Gaussian, μ and σ , and the exponential slope, τ . We generate two distributions (c.f. Fig. 3), the first one corresponding to *light* cosmic-ray

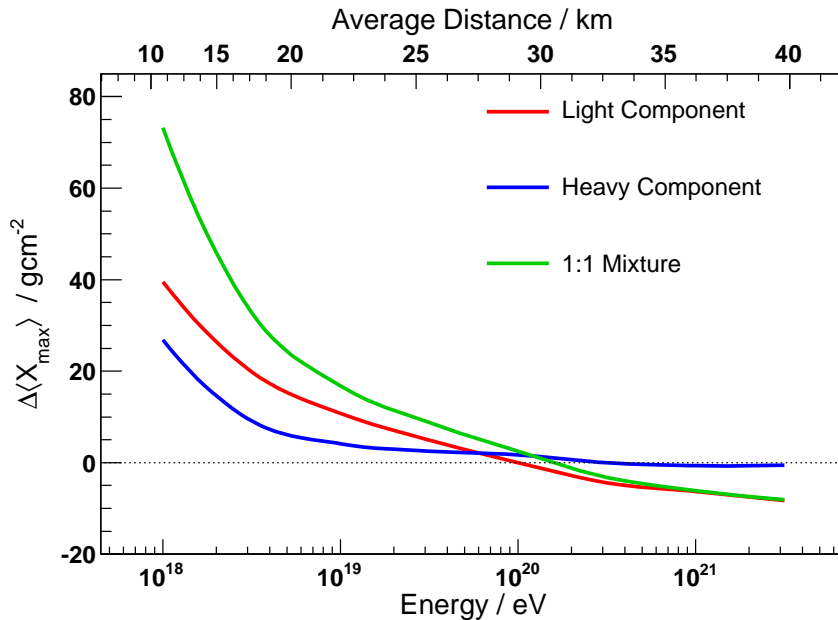


Figure 4: Dependence of the bias $\Delta\langle X_{\max}\rangle$ from the energy and thus the distance of air-showers from the telescope. The upper axis indicates the resulting average distance of showers from the telescope depending on the primary energy.

primaries has an average of 750 g/cm^2 and an RMS of 66.5 g/cm^2 , the second one corresponds to *heavy* cosmic-ray primaries has an average of 650 g/cm^2 and an RMS of 30 g/cm^2 . These values are chosen since they correspond roughly to typical values for proton or iron induced air-showers respectively. The average efficiencies

$$\epsilon_A = \frac{\int_0^{\infty} \left(\frac{dN}{dX_{\max}} \right)_{\text{measured}} dX_{\max}}{\int_0^{\infty} \left(\frac{dN}{dX_{\max}} \right)_{\text{true}} dX_{\max}} = \int_0^{\infty} \epsilon(X_{\max}) dX_{\max}$$

for the observation of X_{\max} with our telescope setup for these two distributions are $\epsilon_{\text{light}} = 33.1\%$ and $\epsilon_{\text{heavy}} = 16.7\%$. The average X_{\max} observed by the telescope setup are $\langle X_{\max} \rangle'_{\text{light}} = 770 \text{ g/cm}^2$ for the light and $\langle X_{\max} \rangle'_{\text{heavy}} = 660 \text{ g/cm}^2$ for the heavy component, which is $10 - 20 \text{ g/cm}^2$ biased with respect to the input distributions. The bias $\Delta\langle X_{\max} \rangle$, de-

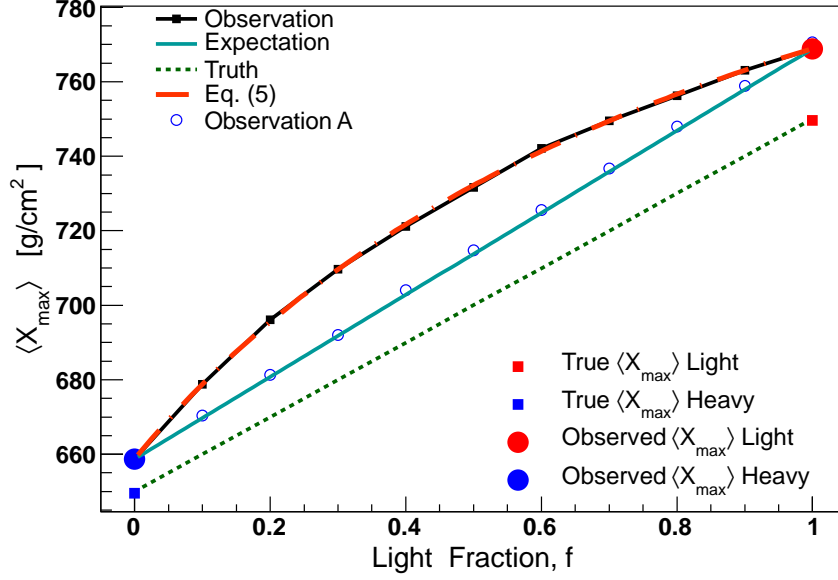


Figure 5: The average X_{\max} as a function of the light cosmic-ray fraction, f . The *observed* $\langle X_{\max} \rangle$ values for pure light and pure heavy compositions are shifted with respect to the *true* $\langle X_{\max} \rangle$. The relation between $\langle X_{\max} \rangle$ and f , and therefore with $\langle \ln A \rangle$ by Eq. 1, is linear for the true X_{\max} distributions, whereas it is non-linear for the case of the observed $\langle X_{\max} \rangle$. The curve labeled “Observation A” indicates the effect on a pure composition of intermediate mass.

defined as the difference between the observed and true $\langle X_{\max} \rangle$ value, changes with distance to the telescope and thus also with the primary energy of the cosmic-ray particles according to Eqs. (2) and (3). In Fig. 4 this is shown for the cases of pure light, pure heavy and an equal mixture of light and heavy primaries. For this study we consider a change of $\langle X_{\max} \rangle$ with energy of $d\langle X_{\max} \rangle/d \lg E = 60 \text{ g/cm}^2$ with respect to the default values used otherwise in this paper. It is interesting to note that the resulting bias depends on the underlying mass composition. In general, for smaller energies the showers are located closer to the telescope and the effect becomes stronger. For example, the low energy fluorescence telescope extensions HEAT [21] at the Pierre Auger Observatory and TALE [22] at the Telescope Array are important to limit these biases by providing a much wider field-of-view for showers at close distances. Furthermore, the bias can be positive as well as negative, depend-

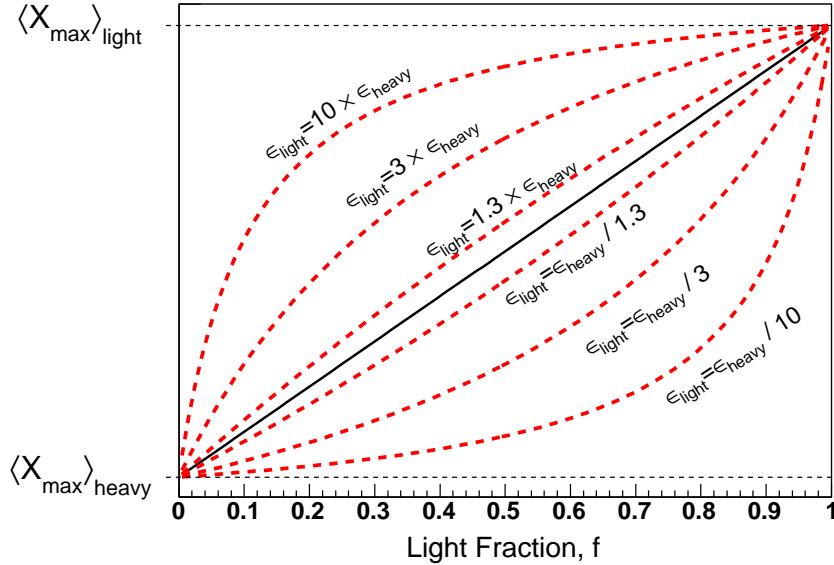


Figure 6: Impact of different values of $r = \epsilon_{\text{light}}/\epsilon_{\text{heavy}}$ on the non-linearity.

ing on the overlap of the true X_{\max} distribution with the telescope efficiency function, c.f. Fig. 2. However, the impact will qualitatively be always as shown in Fig. 4: at short distances the field-of-view cuts shallow showers and thus $\langle X_{\max} \rangle$ is overestimated, at larger distances this effects becomes smaller and eventually might even reverse leading to an underestimation of the true $\langle X_{\max} \rangle$ value. It is important to realize that the primary effect is due to a different distance of showers, and that any parameter that affects the typical observation distance will have a similar impact. Such parameters are typically related to the detector setup, for example the diaphragm opening A_{dia} , the sampling time Δt , but also the atmospheric density profile and optical absorption characteristics.

If we consider a mixture of light and heavy particles at fixed primary energy with a given fraction f of light and $1 - f$ of heavy primary particles, the average observed shower maximum becomes

$$\langle X_{\max} \rangle' = \frac{fr \langle X_{\max} \rangle'_{\text{light}} + (1 - f) \langle X_{\max} \rangle'_{\text{heavy}}}{fr + 1 - f} \quad (5)$$

where $r = \epsilon_{\text{light}}/\epsilon_{\text{heavy}}$. This relation is non-linear in f and thus not in $\ln A$.

In Figure 5 we show the results of this study. The true as well as the observed $\langle X_{\max} \rangle$ are shown, together with the linear interpolation from Eq. (1) and the non-linear version Eq. (5). The latter describes perfectly well the results of our Monte Carlo study.

We also study how a different detector setup affects our result. In general, by changing parameters of the telescope detector setup, very different values of r can be obtained. In Fig. 6 we show how the predictions of Eq. (5) change for a wide range of different values of r . It summarizes the effect described in this paper, and the miss-interpretation it can induce on the inference of the primary mass composition from $\langle X_{\max} \rangle$. For instance, $r = 3$ would imply that a real fraction 50 % proton and 50 % iron, that is $f=0.5$ and $\langle \ln A \rangle = 2$, would be interpreted as 75 % proton and 25 % iron, $\langle \ln A \rangle = 1$, if just the linear relation Eq. (1) is assumed.

4. Summary

The data collected by a fluorescence telescope are affected by acceptance effects, which can have an important impact on the detailed interpretation of the data. This is problematic for researchers not from within a particular experimental collaboration who, for example, have no access to a detailed Monte Carlo simulation of the detector setup.

The average efficiency $\epsilon(X_{\max})$, which describes the response to a flat distribution in X_{\max} , is one of the crucial properties of a fluorescence telescope. However, in addition to the acceptance effects also the detector resolution and X_{\max} reconstruction biases have to be known for a full data analysis.

We have demonstrated that the bias in the average shower maximum introduced by the acceptance of fluorescence telescopes induces a non linearity between $\langle X_{\max} \rangle$ and $\langle \ln A \rangle$.

5. Acknowledgments

We would like to thank A. Olinto for the initial discussions that inspired this work during the TAUP2011 meeting at Munich. J. Bellido, D. Harari, M. Bueno, M. Unger, R. Conceição and M. Pimenta for careful reading of this manuscript and their comments. Finally we thank our colleagues from the Pierre Auger Collaboration for helping us to get the necessary insight on the fluorescence detection techniques. L.C. wants to thank fundings by Fundação para a Ciência e Tecnologia (CERN/FP11633/2010), and fundings

of MCTES through POPH-QREN Tipologia 4.2, Portugal, and European Social Fund.

References

- [1] J. Abraham *et al.* [Pierre Auger Collaboration], Nucl. Instrum. Meth. A **620**, 227 (2010).
- [2] R.U. Abbasi *et al.*, Astropart. Phys. **32**, 53 (2009).
- [3] M. Takeda *et al.* [TA Collaboration], Mod. Phys. Lett. A **23**, 1301 (2008).
- [4] P. Abreu *et al.* [Pierre Auger Collaboration], JCAP **1106**, 022 (2011).
- [5] J. Abraham *et al.* [Pierre Auger Collaboration], Phys. Rev. Lett. **104**, 091101 (2010).
- [6] P. Facal, D. Garcia-Pinto, D. Garcia-Gamez for The Pierre Auger Collaboration, 32nd International Cosmic Ray Conference, Beijing, China, August 2011, arXiv:1107.4804.
- [7] R.U. Abbasi *et al.* [HiRes Collaboration], Phys. Rev. Lett. **104**, 161101 (2010).
- [8] J.N. Matthews [TA Collaboration], Nucl. Phys. Proc. Suppl. **212-213**, 79 (2011).
- [9] D. Ikeda to appear in the proceedings of the 12th international conference of Topics in Astroparticle and Underground Physics, TAUP2011, Munich, 2011.
- [10] J. Abraham *at al.* [Pierre Auger Collaboration], Phys. Lett. B **685**, 239 (2010).
- [11] R. Engel [Pierre Auger Collaboration], AIP Conf. Proc. **1367**, 50 (2011).
- [12] A. Olinto, to appear in the proceedings of the 12th international conference of Topics in Astroparticle and Underground Physics, TAUP2011, Munich (2011).

- [13] M. Unger, B.R. Dawson, R. Engel, F. Schussler, R. Ulrich, Nucl. Instrum. Meth. A **588**, 433 (2008).
- [14] J. Matthews, Astropart. Phys. **22**, 387 (2005).
- [15] J. Alvarez-Muniz, R. Engel, T. Gaisser, J. Ortiz, and T. Stanev, Phys. Rev. D **66**, 033011 (2002).
- [16] M. Unger for the Pierre Auger Collaboration, Nucl. Phys. B (Proc. Suppl.) **190**, 240 (2009).
- [17] E. Ahn *et al.*, Phys. Rev. D **80**, 094003 (2009).
- [18] G.L. Cassiday *et al.*, Astrophys. J. **356**, 669 (1990).
- [19] J. Bellido for the Mass Composition Working Group, Talk at the *International Symposium on Future Directions of UHECR Physics*, CERN, Geneva, 2012.
- [20] R. R. Prado and V. de Souza, *Private communication*.
- [21] H.-J. Mathes for the Pierre Auger Collaboration, 32nd International Cosmic Ray Conference, Beijing, China, August 2011, arXiv:arXiv:1107.4804.
- [22] K. Martens for the Telescopes Array Collaboration, Nucl. Phys. Proc. Suppl. **165**, 33 (2007).